

Enabling Viewpoint Learning through Dynamic Label Generation

MICHAEL SCHELLING, Institute of Media Informatics, Ulm University, Germany

PEDRO HERMOSILLA, Institute of Media Informatics, Ulm University, Germany

PERE-PAU VÀZQUEZ, Universitat Politècnica de Catalunya, Spain

TIMO ROPINSKI, Institute of Media Informatics, Ulm University, Germany

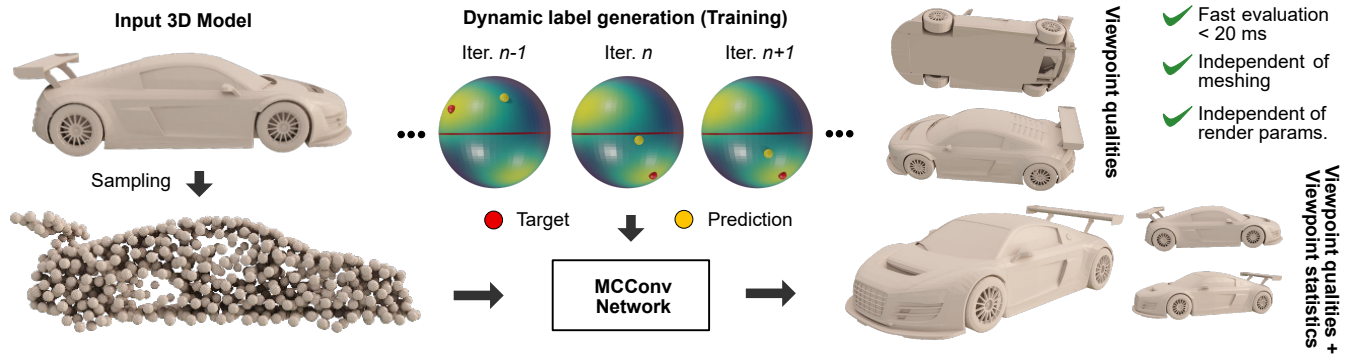


Fig. 1. We propose a new learning-based algorithm which is able to predict high quality viewpoints directly on 3D models. The key to learning viewpoints is our novel dynamic label generation, which resolves inherent label ambiguities and updates the targets of the network during training. This enables our network to learn viewpoints reflecting various viewpoint quality measures, human preference statistics and upright orientation. The use of an unstructured 3D CNN on point clouds makes our approach independent of a rendering engine which allows fast evaluation and makes it robust under different meshings.

Optimal viewpoint prediction is an essential task in many computer graphics applications. Unfortunately, common viewpoint qualities suffer from major drawbacks: dependency on clean surface meshes, which are not always available, insensitivity to upright orientation, and the lack of closed-form expressions, which requires a costly sampling process involving rendering. We overcome these limitations through a 3D deep learning approach, which solely exploits vertex coordinate information to predict optimal viewpoints under upright orientation, while reflecting both informational content and human preference analysis. To enable this approach we propose a dynamic label generation strategy, which resolves inherent label ambiguities during training. In contrast to previous viewpoint prediction methods, which evaluate many rendered views, we directly learn on the 3D mesh, and are thus independent from rendering. Furthermore, by exploiting unstructured learning, we are independent of mesh discretization. We show how the proposed technology enables learned prediction from model to viewpoints for different object categories and viewpoint qualities. Additionally, we show that prediction times are reduced from several minutes to a fraction of a second, as compared to viewpoint quality evaluation. We will release the code and training data, which will to our knowledge be the biggest viewpoint quality dataset available.

Additional Key Words and Phrases: Viewpoint selection, data-driven viewpoint analysis, upright orientation, deep learning, label ambiguity

Authors' addresses: Michael Schelling, Institute of Media Informatics, Ulm University, Ulm, BW, 89075, Germany, michael-1.schelling@uni-ulm.de; Pedro Hermosilla, Institute of Media Informatics, Ulm University, Ulm, BW, 89075, Germany, pedro-1.hermosilla-casajus@uni-ulm.de; Pere-Pau Vázquez, Universitat Politècnica de Catalunya, Barcelona, Spain, pere.pau@cs.upc.edu; Timo Ropinski, Institute of Media Informatics, Ulm University, Ulm, BW, 89075, Germany, timo.ropinski@uni-ulm.de.

1 INTRODUCTION

3D models play an essential role in all areas of computer graphics, such as games, animated movies or virtual reality. To effectively showcase these models or to assess their quality, not only model parameters are important, such as geometry and material, but also the selection of optimal views is crucial. Optimal views should not only ensure that the model complexity is appropriately communicated, and relevant structures are visible, but also that model semantics are considered, by for instance choosing an appropriate up vector which reflects a model's natural orientation, and by reflecting human preferences. Many quality metrics have been developed to aid in the automatic selection of optimal viewpoints on 3D models. The applications range from obtaining vantage points for capturing stills in architecture [He et al. 2017], to initial camera positioning for complex scene inspection [Heinrich et al. 2016; Meuschke et al. 2017; Secord et al. 2011; Song et al. 2014], camera control [Lino and Christie 2015] and recommendations for scientific visualization [Yang et al. 2019].

In this paper, we present the first mesh-based viewpoint learning approach, and demonstrate its applicability by learning different existing viewpoint quality measures as well as the more challenging task of considering viewpoint quality, upright orientation and image statistics at the same time. Thus, we can not only take into account model complexity and relevant structures encoded in information theoretical viewpoint quality measures, but are also able to consider natural orientation and human preferences in order to predict high quality viewpoints for 3D models. We obtain these benefits by shifting the optimization from the rendered image towards the 3D model, which we achieve by exploiting 3D point cloud learning.

To be able to learn high quality viewpoints on 3D meshes, we have developed a novel dynamic label generation, which is used to harmonize labels over the dataset. This is a crucial consideration that needs to be made, as viewpoint quality measures do not necessarily have a unique maximum, but may have several, for instance, but not exclusively, due to model symmetries. Ignoring this ambiguity would lead to conflicting ground truth information, resulting in opposing gradients which prevent meaningful learning. Our two stage label generation process reduces the influence of contradicting label decisions, and thus gradients, by considering the current network predictions to make a unified label decision, in order to learn high quality viewpoints directly on the 3D model.

Since we directly learn on the 3D model, our approach is independent from rendering, which means that on the one hand rendering parameters have no impact on the obtained results, and on the other hand, no rendering engine is required to predict an optimal viewpoint for a given model. Hence, in contrast to previous work, which often optimizes by a brute-force search over a large set of rendered views [Freitag et al. 2015; Kim et al. 2017; Vázquez et al. 2002], our learned approach allows instantaneous predictions. Furthermore, by applying unstructured 3D learning in model space, our approach is also independent of the model’s discretization, which in contrast has a severe impact on conventional viewpoint quality techniques [Bonaventura et al. 2018].

Thus, within this paper we make the following contributions:

- We present the first learning-based approach, that directly predicts optimal views on 3D models, while obeying to different viewpoint quality measures.
- We introduce a novel dynamic label generation method, to tackle label ambiguities inherent to viewpoint learning.
- We release viewpoint quality annotations for a subset of ModelNet40, which makes it the single largest viewpoint quality dataset – by a large margin.

These contributions enable us to learn optimal views directly on 3D geometry and thus enable us to omit an expensive brute-force search over many rendered view alternatives. Our approach further enables an instant prediction of optimal views, by reducing prediction times from several minutes to a fraction of a second. The independence of mesh discretization, enables the prediction of optimal views on a wide range of 3D models from different sources.

2 RELATED WORK

The search for a good viewpoint of a 3D object is a problem that can be dated back to ancient societies such as the Greeks and Romans. Several rules such as the golden ratio, or the rule of thirds have been proposed to estimate beauty or proportion. More recently, the search for preferred views has also been addressed, especially in computer vision tasks (e.g., for object recognition), and researchers have wondered what parameters constitute a good view [Polonsky et al. 2005]. Blanz et al. asked users about their preferences and dubbed preferred views of known objects *canonical views* [Blanz et al. 1999]. They also found that in some cases, these correspond to three-quarter views (also with notable exceptions, such as in the case of vehicles). Secord et al. also analyzed viewpoint preferences

in a large scale user study, and derived a combination of existing techniques [Secord et al. 2011].

Unfortunately, when developing an algorithm to find the best view, the orientation of the objects is commonly unknown, so for instance obtaining three-quarter views from loaded models cannot be done straightforwardly. Thus, algorithms tend to measure elements that are available through the geometry, such as triangles, silhouettes, depth maps, etc.

Viewpoint selection. The automatic selection of viewpoints for 3D scenes has many applications such as helping observers gain understanding on a certain scene [Andújar et al. 2004; Freitag et al. 2017; Liu et al. 2014], for object recognition [Deinzer et al. 2006, 2009], assisting in robotic tasks [Saran et al. 2017], inspection of volumetric models [Meuschke et al. 2017; Mühler et al. 2007; Tao et al. 2009; Vázquez et al. 2008; Viola et al. 2006; Yao 2008], proteins [Heinrich et al. 2016; Vázquez et al. 2002], or scene reconstruction [Marchand and Chaumette 1999; Smith et al. 2018]. Depending on the task to be solved, the algorithms use the available data, sometimes only geometry (e.g., [Lee et al. 2005; Vázquez et al. 2002]), and sometimes combined with user-defined importance (e.g., [Bordoloi and Shen 2005; Mühler et al. 2007]) to define viewpoint quality criteria.

Other researchers focus on combining multiple viewpoint qualities, e.g., with linear regression [Kim et al. 2017; Secord et al. 2011], to reflect the result of user studies. Recently, also deep learning has been used in the creation of saliency maps [Kim et al. 2017] or to score candidate viewpoints [Yang et al. 2019]. Discussing the dozens of such techniques would be beyond the scope of this work, and thus we would like to guide the interested reader to some of the comparisons that have been published in literature [Bonaventura et al. 2018; Freitag et al. 2015; Secord et al. 2011].

Despite the number of articles devoted to this issue, little has been done to generate fast algorithms for good viewpoint selection. In most cases, the metrics require inspecting a very dense set of candidate views, which is time consuming. Accelerations presented in literature are typically greedy algorithms (e.g. for light source positioning [Gumhold 2002], or for volumetric models [Monclús et al. 2012]). Our learned viewpoint prediction outperforms all these methods by design, as one forward pass through the network enables viewpoint prediction in milliseconds, rather than minutes, which are required by the brute-force approaches. Furthermore, we can also consider upright orientation and human preferences, without additional costs.

User preferred views. As mentioned before, prior research has focused on the user preferences when selecting viewpoints of objects [Blanz et al. 1999; Secord et al. 2011]. However, user experiments are time consuming and can be usually carried out only on a limited number of participants [Tamboli et al. 2018]. Accordingly, researchers have turned to automation to extract user preferred views from existing data. This can be done by computing similarities between images and candidate viewpoints of 3D models [Liu et al. 2012], through a clustering strategy to recover viewpoints for architectures [He et al. 2017], or by using a CNN viewpoint estimator to retrieve viewpoint probabilities from publications for medical data [Shi and Tao 2019]. In contrast to these approaches,

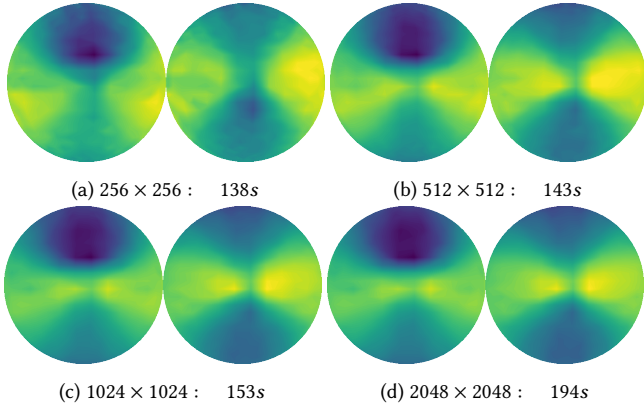


Fig. 2. **Influence of image resolution.** Projection of VE on the viewpoint sphere from $\pm y$ -axis for model *airplane_0275* from ModelNet40 computed at resolutions 256Åš, 512Åš, 1024Åš, 2048Åš and the time needed to sample the viewpoint sphere \mathcal{V} , averaged over 10 runs. We choose a resolution of 1024Åš as a trade-off between accuracy and speed. Note that the locations of the maxima (yellow) are stable at higher resolutions.

we propose to combine a data-driven elevation distribution estimation from images with information theoretical viewpoint quality measures.

Up vector prediction. Several methods were proposed to orient 3D models, many of them rely on handcrafted features, such as PCA [Kazhdan et al. 2003] or the convex hull [Fu et al. 2008; Kim et al. 2017; Lin and Tai 2012]. Deep neural networks on the other hand are able to incorporate both feature extraction and prediction at the same time, for example on voxelized models [Liu et al. 2016]. Our model instead, directly predicts upright orientation using 3D convolutions on unstructured point clouds, which does not require an additional discretization of the input space.

Label ambiguity. While classification tasks can resolve label ambiguity by design, regression tasks often struggle with ambiguous label information. While restating a regression problem as a classification problem is possible [Shi and Tao 2019], it limits the possible performance by discretizing the output space. Only partial restatement can though be a trade-off in some cases, e.g., to resolve axial symmetry [Liao et al. 2019] or rotational symmetry [Corona et al. 2018]. In contrast to these approaches, we present a novel dynamic label generation, which harmonizes labels during training without further assumptions or restrictions.

3 TRAINING DATA GENERATION

Before introducing our learning method, this section first briefly describes the training data generation process, which we had to perform as available viewpoint data is too limited for our purposes. To generate the data, we evaluated different viewpoint quality metrics on preprocessed 3D meshes and, in order to also consider measures that do not only depend on the model geometry, we combine them with human preference analysis from images.

3.1 Viewpoint Quality Measures

To demonstrate the proposed deep learning technology, we learn four different viewpoint quality measures: the Visibility Ratio (VR) [Pleminos and Benayada 1996], the Viewpoint Entropy (VE) [Vázquez et al. 2001], the Viewpoint Kullback-Leibler divergence (VKL) [Sbert et al. 2005] and the Viewpoint Mutual Information (VMI) [Feixas et al. 2009], which are defined as:

$$\text{VR} = \sum_{z \in \mathcal{Z}} \text{vis}_z(v) \frac{A_z}{A_t}$$

$$\text{VE} = - \sum_{z \in \mathcal{Z}} \frac{a_z(v)}{a_t(v)} \log \frac{a_z(v)}{a_t(v)}$$

$$\text{VKL} = \sum_{z \in \mathcal{Z}} \frac{a_z(v)}{a_t(v)} \log \frac{a_z(v)A_t}{a_t(v)A_z}$$

$$\text{VMI} = \sum_{z \in \mathcal{Z}} p(z|v) \log \frac{p(z|v)}{p(z)},$$

where we follow the notation of Bonaventura et al. [Bonaventura et al. 2018]:

z	polygon
\mathcal{Z}	set of polygons
$\text{vis}_z(v)$	visibility of polygon z from viewpoint v (0 or 1)
$a_z(v)$	projected area of polygon z from viewpoint v
$a_t(v)$	projected area of the model from viewpoint v
A_z	area of polygon z
A_t	total area of the model
$p(z v)$	conditional probability of z given v
$p(z)$	probability of z

The best viewpoints for VR and VE correspond to the highest viewpoint quality values, and for VKL and VMI to the lowest viewpoint quality values. These viewpoint quality measures are defined for polygonal models and thus are, in contrast to our approach, dependent on the actual meshing with various degrees. While VR and VMI are insensitive to the discretization of the model, and VKL is near insensitive, they all still assume clean surface meshes, as for example self-intersections of polygons change A_t and A_z and thus also VR and VKL, without necessarily altering the visible surface. These inconsistencies make it harder to compare good viewpoints for models under different meshing qualities or resolutions, which is a problem if we want to extract model-spanning features of good viewpoints. Thus, we employ a pipeline to clean meshes (see Section 3.4), in order to achieve comparable viewpoint quality computations for different meshes.

To generate our training data, we sample the unit sphere with 1k viewpoints $\mathcal{V} \subset \mathbb{R}^3$ on a Fibonacci sphere [González 2010], generating almost equidistantly distributed viewpoints, for which we compute the four viewpoint quality measures. After evaluating the resolutions shown in Fig. 2, we chose to render the 3D meshes with 1024 × 1024 pixels, where the camera is placed at a distance of half the diagonal of the bounding box, centered on the mean of the bounding box, using perspective projection. We found this a good

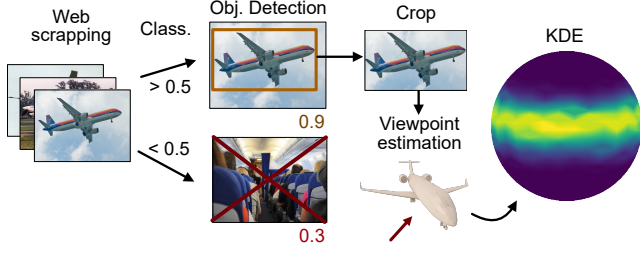


Fig. 3. **Viewpoint estimation pipeline.** Overview of the applied approach to extract viewpoint statistics from images. We collected images from popular image hosting sites to be processed by an object detection network. Images with a classification score below 0.5 are dropped, the rest is cropped to the predicted bounding boxes and processed by a viewpoint estimation network. The density distribution of the extracted elevations is then estimated using a kernel density estimation (KDE).

trade-off in accuracy and compute time. We further normalized each measure to the range $[0, 1]$, where 0 and 1 refer to the viewpoint quality of the worst and best viewpoint, respectively:

$$VQ^*(v) = \frac{VQ(v) - VQ(v^-)}{VQ(v^+) - VQ(v^-)},$$

where $v^+ \in \mathcal{V}$ is a viewpoint with the best and $v^- \in \mathcal{V}$ one with the worst viewpoint quality of the sampled views \mathcal{V} . In the following we will always refer to these normalized versions of the viewpoint quality measures.

3.2 Viewpoint Statistics

The viewpoint qualities described above, only measure the informational content of an image, derived from the model geometry, in order to evaluate the amount of visual information it carries. Thus, they might result in theoretically informative but visually unpleasant or unnatural views. While standard brute-force view quality measures have limitations with the latter two, learning does naturally support their integration. Accordingly, we decided to also bring in relevant training data. To estimate user preferences on viewpoint selection we collected data from popular image hosting sites and retrieve the viewpoints from those images (see Fig. 3).

The images are collected by choosing the top $1k$ images return by a search for a given category name (e.g., plane or chair) from www.flickr.com. The resulting images are then processed by the YOLOv3 object detection approach [Redmon and Farhadi 2018], which we used to create bounding boxes and classification scores. Objects with a classification score below 0.5 are dropped whereby the object detection also serves as a filter for unwanted images, e.g., images showing the inside of a plane. All objects passing the filter are cropped from the images, where we allow multiple objects per image to pass. To retrieve the viewpoints from the processed images we use a S_{exp}^1 spherical regression network [Liao et al. 2019] and retrain category specific instances of this network to further boost the performance and increase the higher level accuracy scores, details can be found Appendix A.

At this point it would be possible to analyze the distribution on the viewpoint sphere and search the point of highest density, which would arguably be a viewpoint of high user preference. However,

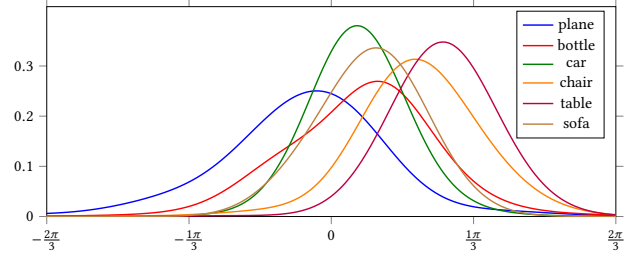


Fig. 4. **Elevation densities.** Comparison of elevation KDE results for different Pascal3D+ categories on images from flickr.

this viewpoint would be category specific, not taking into account differences of distinct instances of these categories. Thus, we follow the findings of Blanz et al. [Blanz et al. 1999], who state that there is a preference towards certain elevations of the viewpoint and only analyze the extracted elevations. Accordingly, we estimate the elevation distribution of the collected images by performing a kernel density estimation (KDE) on the extracted elevations \mathcal{E} using a Gaussian kernel k :

$$\tilde{f}(x) = \frac{1}{nh} \sum_{e \in \mathcal{E}} k\left(\frac{x-e}{h}\right),$$

$$k(t) = \frac{1}{\sqrt{2\pi}} \exp(-t^2).$$

To account for inaccuracies in the viewpoint estimation routine we set the kernel bandwidth h to 0.05π . The resulting elevation densities can be seen in Fig. 4, confirming the 'slightly above horizon' preference described by Blanz et al. [Blanz et al. 1999] for most categories.

In order to ensure that our model inherits no significant bias from the used image source we performed a second density estimation on an independent image set obtaining similar results, details can be found in Appendix B.

3.3 Combined Viewpoint Quality Measures

Previous work on combining viewpoint quality measures and statistics [Kim et al. 2017; Secord et al. 2011] proposed using linear combinations to model human preference, however this approach possibly still assigns high qualities to unnatural views, i.e., views not present in the statistics. To exclude such views and capture both informational content and data-driven user preference, we propose the combined viewpoint qualities

$$(VQ + S)(v) = VQ^*(v) \cdot \tilde{f}(e_v),$$

where VQ^* is a normalized information theoretic viewpoint quality measure as described in Section 4.1 and e_v is the elevation of the current viewpoint v , with respect to the model's up vector. This way, the viewpoint quality is considered 0 for views not observed in the data.

3.4 Mesh Cleaning

As mentioned above, some viewpoint quality measures are sensitive to the meshing of the models, and bad meshing qualities can lead to

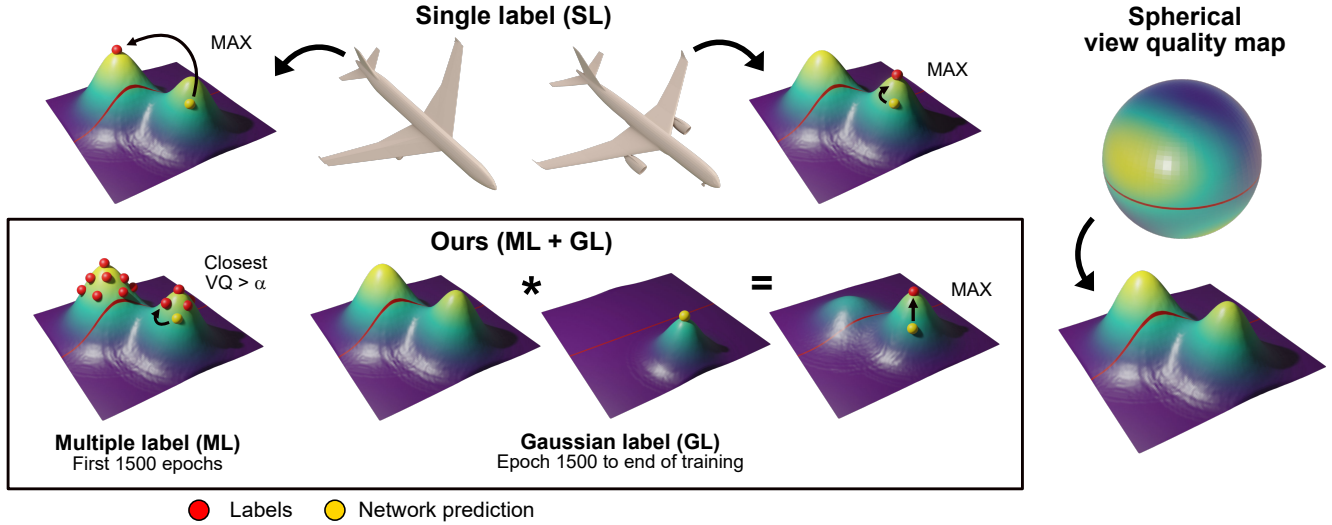


Fig. 5. **Dynamic label generation.** Illustration of the proposed dynamic label generation technique. *Top*: Best viewpoints are not necessarily unique, thus randomly choosing a maximum as label can create different labels for similar input models, which the network is unable to resolve. *Bottom*: To harmonize the label decision, we propose our two stage dynamic label generation. We first provide the network with multiple labels (ML) of high viewpoint quality and optimize towards the closest one. The labels typically form clusters in high quality areas, in which case the optimization is towards the boundary. To refine the predictions, we generate the label dynamically during training stage two (GL). For this the viewpoint quality distribution is weighted with a Gaussian centered at the current prediction. We choose as label the maximum of the result, which is typically a close local maximum, i.e., the maximum of the closest cluster. Both stages, ML and GL, provide more similar labels for similar input. For illustrative purposes, we use Mercator projections of the viewpoint sphere, as indicated on the left.

inaccuracies in the viewpoint quality computation. These inaccuracies reduce the comparability between different models, which makes it hard for a network to determine the important features. To minimize these influences, we pass all meshes through a mesh cleaning pipeline, which resolves mesh intersections and regularizes the meshing. For details on the mesh cleaning and its influence on the viewpoint quality measures we refer the user to Appendix C.

4 HIGH QUALITY VIEWPOINT PREDICTION

Predicting good viewpoints with neural networks confronts us with two major challenges, the mesh dependency of the viewpoint qualities and the non-uniqueness of the best viewpoint. To reduce the impact of the mesh quality we apply the aforementioned mesh cleaning pipeline, resulting in a comparable polygonization of all meshes. To resolve the label ambiguity we propose to apply our novel dynamic label generation approach during training. Additionally, to provide the correct in plane rotation when rendering the models, we train a separate network to predict the upright orientation.

4.1 Dynamic Label Generation

As viewpoint quality measures do not necessarily have a unique maximum, e.g., due to symmetry in the 3D model, one has to make a decision which viewpoint to provide as ground truth to the network. The naïve approach would be to ignore label ambiguity and choose one viewpoint v^+ with a viewpoint quality of 1 as the Single Label

(SL) for each model and train to minimize the cosine distance

$$\begin{aligned} \ell(\hat{v}) &= 1 - \frac{\hat{v} \cdot v^+}{\|\hat{v}\|_2 \|v^+\|_2} \\ &= 1 - \hat{v} \cdot v^+, \end{aligned}$$

between the prediction \hat{v} and the best viewpoint. (Note: ℓ_2 norms are 1 as we evaluate on the unit sphere.) However, if this decision is not consistent over the entire dataset, the network is unable to resolve the label ambiguity during training, e.g., if two similar models are labeled with different best viewpoints, both having high viewpoint quality for both models, the networks receives contradicting gradients impacting the learning capability, as illustrated in Fig. 5 (*top*).

We address this problem by proposing our novel, dynamic label generation approach, which is applied during training to harmonize label decisions over the dataset. Our approach makes two critical advances over the single label approach. First, it facilitates the use of multiple labels, and second, it generates labels dynamically, by means of a low pass filtering, in order to guide the search. In the following paragraphs, we described these two advances, which we combine during training for best performance.

Multiple Labels (ML). Our first step towards addressing label ambiguity, is to select a set of good viewpoints \mathcal{V}^+ as labels, where we define a good viewpoint through having a viewpoint quality in a 1% range from the optimal value 1

$$\mathcal{V}^+ := \{v \in \mathcal{V} \mid VQ^*(v) \geq 0.99\}.$$

During training we aim to minimize the cosine distance to the closest label in \mathcal{V}^+

$$\ell(\hat{v}) = \min_{v \in \mathcal{V}^+} (1 - \hat{v} \cdot v).$$

In practice \mathcal{V}^+ often consists of clusters covering areas of good viewpoint quality values, which are similar if the input models are similar, causing the gradients to reinforce each other. However, as the network only optimizes to the closest label, we observe it stopping at the boundary of one of these clusters, rather than moving towards its center (see Fig. 5), which results in non optimal values. To further improve the performance we propose a second stage, which refines the predictions.

Gaussian Labels (GL). In order to keep optimizing towards the closest high quality viewpoint while still aiming at the optimal position inside a promising region, we propose the combination with Gaussian labels in order to resolve label ambiguity. Thus, during training we generate labels dynamically depending on the current prediction, which guides the network to the optimal position. We incorporate this by multiplying the viewpoint quality measure by a shifted Gaussian function

$$VQ_g(v, \hat{v}) = VQ^*(v) \cdot \left(\exp \frac{\|v - \hat{v}\|_2}{8} + 1 \right),$$

and then optimize towards the viewpoint with highest value in this measure

$$v_g^+(\hat{v}) = \operatorname{argmax}_{v \in \mathcal{V}} VQ_g(v, \hat{v}),$$

$$\ell(\hat{v}) = 1 - \hat{v} \cdot v_g^+(\hat{v}),$$

as illustrated in Fig. 5. The Gaussian function lays an emphasis on good viewpoints which are closer, effectively choosing similar viewpoints as labels for similar models. The additive term of 1 to the Gaussian function ensures that distant good viewpoints are not dismissed, which keeps the network from getting stuck in larger regions of bad viewpoint qualities.

When solely applying this approach, it will keep optimizing towards a local maximum of VQ_g , whereby the value of this local maximum can be in some cases sub-optimal, if the initial guess of the network is in a bad region. Thus, we are using ML for initialization in order to improve the obtained results.

To succeed, we combine the strengths of the ML and GL approaches and employ a two stage training, where we first train with ML optimizing the network towards the best viewpoints \mathcal{V}^+ . In the second stage, we train with GL, refining the predictions with the goal of moving them towards the local maximum inside the clusters.

4.2 Data Augmentation

Neural networks working with three dimensional input data usually require a large database to achieve noteworthy performance. This is due to the high dimensionality of the input space, as well as to the complexity of the task. As the available sources for 3D data are rather limited, as compared for example to image data, the use of data augmentation, which increases the dataset virtually, are crucial for our experiments.

Therefore, we use the following three data augmentation strategies:

Rotations. If not specified otherwise we augment the data with rotations from $SO(3)$, whereby the three angles are chosen from a random uniform distribution on $[0, 2\pi]$.

Noise. We further add white Gaussian noise to the vertex coordinates, where we use 0.01 of the size of the bounding box as variance and clip the noise at 0.02 of the size of the bounding box.

Symmetry preserving deformations. While the previous two methods do increase the size of the dataset, they do not alter the model geometry fundamentally. Therefore, we also use symmetry preserving deformations similar to Sederberg et al. [Sederberg and Parry 1986], in order to increase the model variety in the training dataset. For details about the implementation we refer to Appendix D.

As mentioned beforehand, the viewpoint quality measures are insensitive to in plane rotations but noise and deformations change the model geometry, thus we only use rotations for data augmentation for the viewpoint prediction networks. The up vector prediction network uses all three techniques during training.

4.3 Network Architecture

To learn viewpoint qualities, we make use of Monte-Carlo Convolutional Neural Networks (MCCNN) [Hermosilla et al. 2018], which implement hierarchical 3D convolutions. They enable the detection of model properties at different scales, which is crucial for our task. Our network consists of four convolutional layers with convolutional radii 0.05, 0.2, 0.3, $\sqrt{3}$, relative to the bounding box of the model. Each convolutional layer operates on different resolutions, which are computed using Poisson disk sampling with radii 0, 0.025, 0.1, 0.4, $\sqrt{3}$, again relative to the bounding box of the model. The respective feature dimensions are 3, 128, 256, 1024, 2048, and the resulting architecture is shown in Fig. 6 (top). After the convolutional layers, we add four parallel Multi Layer Perceptrons (MLPs) with three layers of sizes 1024, 256, 3, each outputting a viewpoint $\hat{v} \in \mathbb{R}^3$ for one of the four viewpoint quality measures. We found that predicting all four viewpoints with one network actually leads to better results as compared to training four separate networks. An effect we account to the different losses improving the feature extractor, similar to auxiliary losses [Szegedy et al. 2015].

For all conducted experiments, we used the same hyperparameters, stressing that our network is applicable to different categories and viewpoint quality measures without further tuning. Namely we use dropout [Srivastava et al. 2014] in the MLP layers with a dropout rate of 0.5 and an Adam optimization [Kingma and Ba 2014] with batch size of 8 and a learning rate decay with an initial learning rate of 0.001 which is multiplied by 0.75 every 200 epochs. We train for a total of 3000 epochs and switch from ML to GL after 1500.

5 EXPERIMENTS

To validate our viewpoint learning approach, which is enabled by dynamic label generation, We conducted five experiments. First, we trained a neural network to predict good viewpoints on point clouds of arbitrarily oriented 3D models, while we compare our label generation method to existing techniques. To orient the 3D models along a natural orientation we conducted a second experiment for up vector regression. Third, we evaluated our network when

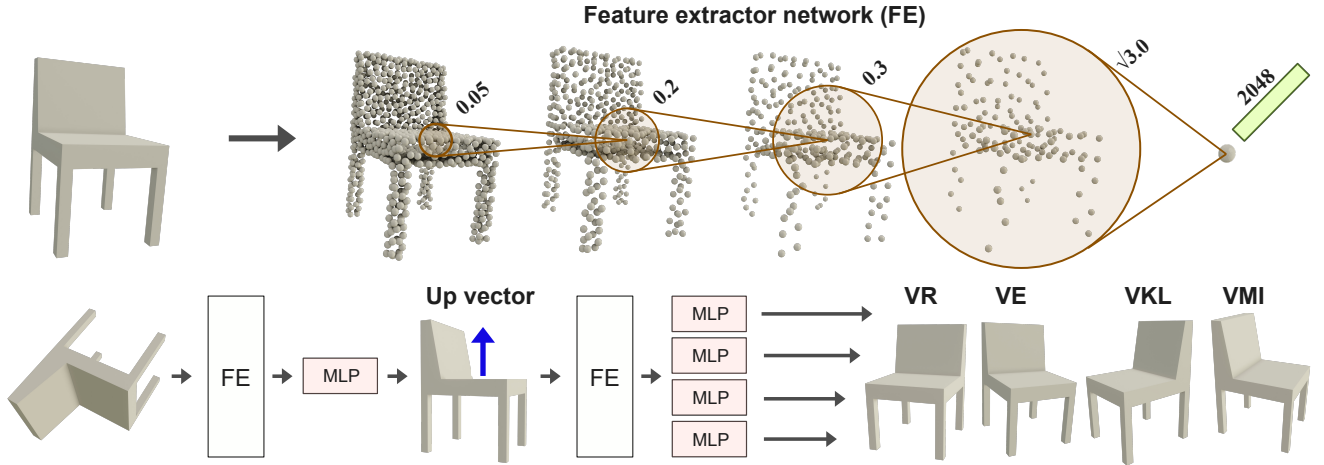


Fig. 6. **Overview of the proposed network architecture.** *Top:* We use a four layer MCCNN as a feature extractor, each layer performs a spatial convolution with increasing radius which increases the feature dimension gradually up to 2048 and reduces the spatial resolution. *Bottom:* For learning $VQ + Statistics + Up$ we employ two separate networks for predicting the up vector and the viewpoints, which are trained independently. During testing first the up vector is predicted which is used to align the 3D model before predicting the viewpoints for the different viewpoint quality measures.

predicting high quality views in our combined viewpoint qualities VQ s while simultaneously aligning the model to an upright orientation. Next we inspected the robustness of our method towards different meshing and samplings of the input models, and lastly provide timings for both the sampling algorithm and our network.

5.1 Data

All experiments were conducted on a subset of ModelNet40 [Wu et al. 2015], composed of the categories *airplane*, *bench*, *bottle*, *car*, *chair*, *sofa*, *table* and *toilet*, which we split into 80% training, 10% validation and 10% test data. All models were preprocessed as described in Section 3.4. In order to sample the viewpoint quality measures in reasonable time we only use models with at most 10k faces. For the combined viewpoint quality measures $VQ+S$ we matched categories of Pascal3D+ and ModelNet40, whereby we set *bench* as *sofa* and *toilet* as *chair*.

All meshes were converted into point clouds by sampling 20k random uniform points on the faces. The input point clouds were generated by selecting 1024 points using farthest point sampling [Eldar et al. 1997], and selecting additional random points until we reach the desired input size.

5.2 Viewpoint Prediction

We demonstrate the effectiveness of our two stage dynamic label generation (ML+GL) by comparing it against single label cosine-distance (SL) and existing work on resolving label ambiguity, Spherical Regression (SR) [Liao et al. 2019], which splits the optimization into two parts, a regression for the absolute value $|v|$ and a classification task for the signs. The loss function ℓ for SR consists of the cosine distance to $|v^+|$ and the cross entropy-loss of the sign prediction.

We train a MCCNN as described in Section 4.3 on each category to predict four different viewpoint quality measures, the Visibility

Ratio (VR), the Viewpoint Entropy (VE), the Viewpoint Kullback-Leibler divergence (VKL) and the Viewpoint Mutual information (VMI). (Note: For SR we use two MLPs per output to predict absolute values and the sign categories.) As input data we choose a higher number of points, 4096, to capture finer geometric details in the models. We measured the mean viewpoint qualities of the predicted viewpoints on the test set, averaged over all categories, and compared the different methods in Table 1. Our proposed two stage combination of ML and GL (ML+GL) clearly outperforms the naïve approach SL and SR, confirming that our proposed method provides a better way to resolve label ambiguity for this task.

We found that SR is not always able to resolve the ambiguity leading to predictions with wrong sign decisions or false regression results for $|v|$, interpolating good viewpoints, see Fig. 8. We theorize that this is because an underlying assumption for SR is that $|v|$ is the same for all labels, but as in our case the label ambiguity does not solely stem from model symmetry and the input is not necessarily aligned with the 3D axes, the assumption does not hold.

Further, we performed an ablation study where we compare our combined ML+GL approach to only using multiple labels (ML) and Gaussian labels (GL), see Table 1. The two stage ML+GL method improves over both single stage methods. We conclude that initializing the predictions with ML substantially improves the results over training solely with GL, as GL has a stronger locality restriction, making it sensitive to initialization.

The results of our method are stable for all examined categories as can be seen in the bottom half of the table, showing that no additional tuning of the hyperparameters is necessary to learn various categories or viewpoint quality measures, detailed results can be found in Appendix F.

Viewpoints predicted on the test set, i.e. unseen models, by our network trained with ML+GL labels can be seen in Fig. 7. We stress that due to label ambiguity the network is not optimized towards

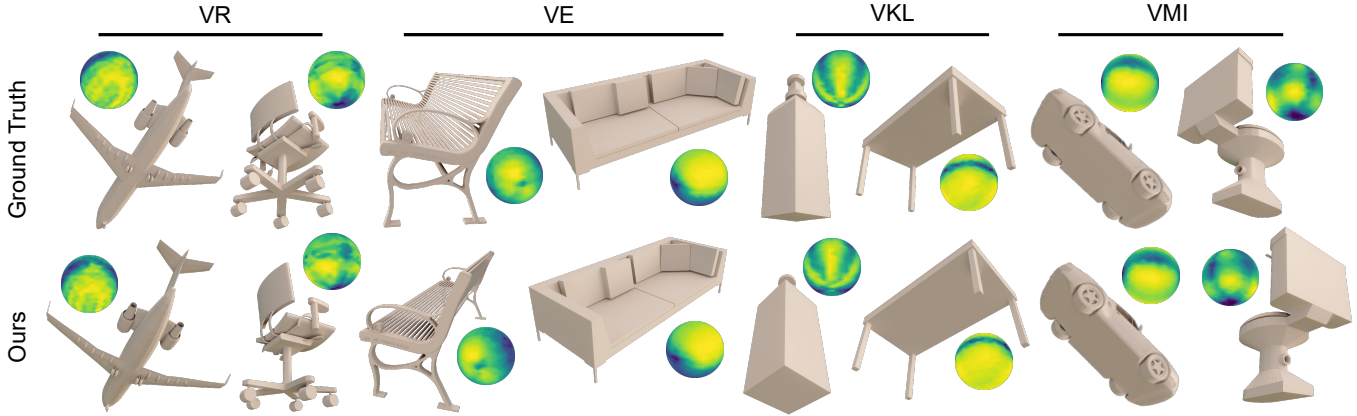


Fig. 7. **Viewpoint prediction results for different viewpoint qualities.** Viewpoints predicted by our network for unseen models and ground truth achieved from sampling the viewpoint sphere. We also show the corresponding viewpoint quality spheres centered at the displayed viewpoint. The network successfully predicts high quality viewpoints, indicated by the yellow areas in the viewpoint spheres.

reproducing the same viewpoint as the sampling method, but to predict a viewpoint with high viewpoint quality. This potentially leads to different views, e.g., the toilet in Fig. 7, for which the views also have a high quality, as can be seen in the viewpoint quality spheres in the figure.

5.3 Upright Orientation Estimation

As the viewpoint qualities do not account for model orientation, we train an additional MCCNN to predict the up vector. As input data we use 1024 points, we found that this lower number of points results in a better generalization, and use rotations, noise and deformations for data-augmentation. We train the network with SL as we have a unique label in this task.

The network achieves an average accuracy of 88% at $\pi/6$ and a mean cosine distance of 0.07 on the test set. For detailed results on the different categories as well as a comparison to using SR labels we refer the reader to Appendix E. Predicted upright orientations can be seen in the second row of Fig. 9.

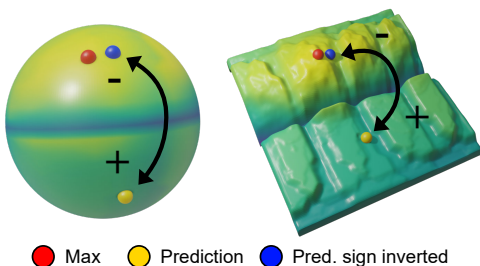


Fig. 8. **Spherical regression.** SR struggles with resolving label ambiguity as the ambiguity is not axisymmetric leading to predictions that have flipped sign decision (yellow) although the absolute value might be correct (blue).

5.4 Prediction for Combined Viewpoint Qualities

Predicting the $VQ+S$ viewpoint qualities is a more complex problem, as the network has to learn the orientation of the model and find good views in a specific range of elevations. This lowers the quality of the predictions as can be seen in Table 2 in row $SO(3)$. We exploit this natural decomposition of the task and use the network from the previous experiment 5.3 to predict the up vector and train a separate network to predict the viewpoints on the aligned models. We mimic the upright correction by applying arbitrary rotations only around the up vector and account for inaccuracies in the up vector prediction by adding small rotations in the other axes according to

Table 1. **Viewpoint prediction results.** *Top:* Mean viewpoint quality in % of the predicted viewpoints using the different labeling techniques on the test set. Our proposed two stage dynamic label generation method ML+GL yields best results for all four viewpoint quality measures, improving over one stage methods (ML, GL) and existing methods (SL,SR). *Bottom:* Mean viewpoint quality in % of the ML+GL approach for the different categories. The performance is consistent over all categories.

labels	categories	VR	VE	VKL	VMI
SL	mean	71.0	62.4	80.7	83.0
SR	mean	69.8	63.1	80.6	80.1
Ours (ML+GL)	mean	78.2	79.3	91.2	92.5
Ablation 1 (ML only)	mean	72.1	70.1	82.6	82.1
Ablation 2 (GL only)	mean	75.1	74.2	89.3	87.7
Ours (ML+GL)	airplane	74.8	79.1	95.2	96.6
Ours (ML+GL)	bench	72.8	67.7	85.5	87.3
Ours (ML+GL)	bottle	78.0	75.3	94.9	94.1
Ours (ML+GL)	car	80.3	84.0	89.7	92.2
Ours (ML+GL)	chair	77.9	73.0	90.8	93.0
Ours (ML+GL)	sofa	75.7	88.8	92.2	93.5
Ours (ML+GL)	table	82.0	83.0	91.6	90.1
Ours (ML+GL)	toilet	84.3	83.8	89.8	93.4

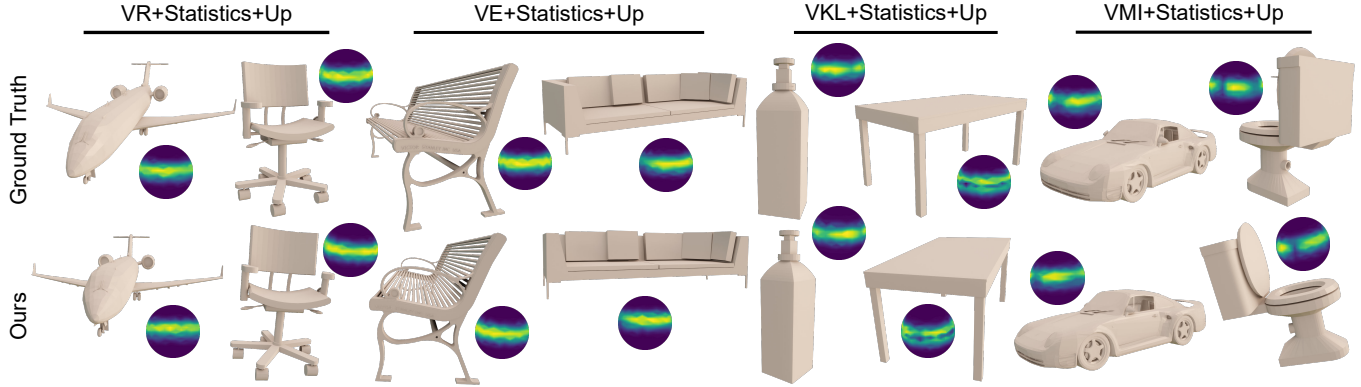


Fig. 9. **Viewpoint and upright prediction results for our combined viewpoint qualities.** Viewpoints predicted by our network and ground truth for unseen models. We also show the corresponding viewpoint quality spheres centered at the displayed viewpoint. The network successfully restores the upright orientation and predicts high quality viewpoints, indicated by the yellow areas in the viewpoint spheres.

a clipped Gaussian normal distribution with variance 0.15 which we clip at a magnitude of 0.45. We train the network independently of the up vector prediction network and only concatenate them during testing. Apart from the rotations we use the same training setting as in Section 5.2. The approach is illustrated in Fig. 6 (bottom), whereby we report its test results in Table 2 in row $SO(3)$, *pred. up*. Resulting views, including upright orientation correction, on unseen models are shown in Fig. 9. We would like to emphasize, that the network might predict high quality viewpoints which are different to the best viewpoints of the sampling method, e.g., for the shown toilet mesh. While correcting the up vector increases the

performance the network still does not reach the same performance as on the unaltered viewpoint quality measures as in Section 5.2. The reason for this is, that the areas of high viewpoint quality are narrower, especially the range of elevations, which can be seen in the viewpoint quality spheres shown in Fig. 9. Thus, a small error in the models' upright orientation can reduce the viewpoint quality drastically. As a consequence, fixing the up direction during training and only rotating around the up vector, the performance can be further increased, see row *fixed up* in Table 2, confirming that the source of the performance loss is located in the upright orientation prediction. Detailed results can be found in Appendix F.

By comparing the results of our network to the views obtained from sampling the viewpoint qualities, see Fig. 10, we see that the network successfully predicts more natural elevations, provided by our elevation statistics.

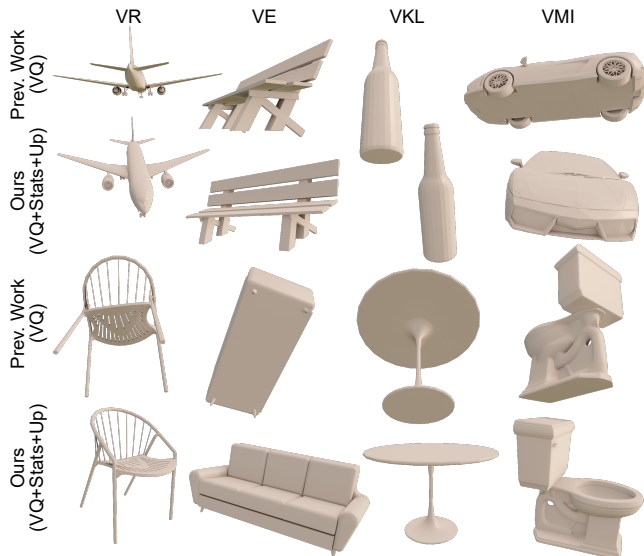


Fig. 10. **Influence of elevation statistics.** Comparison of standard viewpoint qualities to our network on unseen models. As the network learns a combination of viewpoint qualities and image statistics the resulting viewpoints reflect human viewpoints on objects better.

Table 2. **Viewpoint prediction results for our combined viewpoint qualities.** Viewpoint quality measure $VQ+S$ test results in % for ML+GL on: arbitrarily rotated models ($SO(3)$), models aligned with predicted upright direction (*pred. up*), and models in correct upright direction (*fixed up*).

input	category	VR + S	VE + S	VKL + S	VMI + S
$SO(3)$	mean	67.3	73.3	65.8	65.0
$SO(3)$, pred. up	mean	78.0	83.2	78.5	77.0
fixed up	mean	88.1	93.1	87.8	87.1
$SO(3)$, pred. up	airplane	87.7	92.2	86.8	88.0
$SO(3)$, pred. up	bench	79.4	73.6	66.3	67.7
$SO(3)$, pred. up	bottle	86.6	90.3	90.6	90.7
$SO(3)$, pred. up	car	70.7	92.6	82.1	79.3
$SO(3)$, pred. up	chair	81.6	83.2	78.8	78.5
$SO(3)$, pred. up	sofa	76.2	84.8	83.4	82.0
$SO(3)$, pred. up	table	80.3	82.1	76.1	73.6
$SO(3)$, pred. up	toilet	62.0	66.6	64.0	55.9

Table 3. **Robustness to input sampling.** Comparison of the network performance for different input data: *preprocessed*: by our mesh cleaning pipeline, *raw*: from unaltered ModelNet40, *surface*: point sampling of Qi et al. [Qi et al. 2017]. The network achieves comparable results under different input meshing and point sampling methods.

source	VR	VE	VKL	VMI
preprocessed meshes	78.2	79.3	91.2	92.5
raw meshes	76.2	78.9	88.6	90.4
surface sampling	74.6	79.1	88.9	88.4

5.5 Mesh and Sampling Independence

We use unstructured 3D convolutions and hence the input to the network are point clouds only consisting of coordinate information. As these points carry no additional information about the polygonization of the underlying mesh we expect our approach to be insensitive to the discretization of the mesh.

To confirm this we perform two different experiments. The first one is the application to a toy example, in which we subdivide a part of the *chair_0047* mesh into smaller polygons. On the original model the viewpoint entropy VE prefers views from the bottom showing more geometric details in form of the legs, while after subdividing the seating surface the viewpoint entropy VE mistakes the small faces as surface details, emphasizing the visibility of this area, see Fig. 11. Our approach on the other hand, predicts viewpoints in an optimal area of the original mesh, independent of the meshing.

To verify this robustness in practice, we tested our network on the raw ModelNet40 models, which contain self-intersections, non-surface faces and non-uniform discretization, to additionally show independence of the point sampling strategy we also evaluate on the points provided by Qi et al. [Qi et al. 2017], who use a different pipeline to achieve clean surface point clouds. The results reported in Table 3 confirm that our approach is robust under sampling of the input data. We infer that the network has learned an internal representation of the meshing used during training.

5.6 Timings

We compared the time needed to estimate high quality viewpoints using the sampling approach described in Section 3.1, and the time needed to predict high quality views using our neural network model, as described in Section 4.3. The timings were measured on a system with an Intel Core i7-8700K CPU @ 3.70GHz and a NVIDIA GeForce GTX 1080 GPU. While the sampling approach was implemented using Python and OpenGL, our network approach was realized through Python and TensorFlow. To make the measurements comparable, we employed the following two conditions. First, we neglected initialization times, which include loading the meshes, preprocessing the meshes for the sampling method and sampling points and loading the weights for the network. Second, we sampled the viewpoint quality measures in one procedure, computing shared values only once. For the evaluation we chose models of different sizes, ranging from 10k faces to 1M faces, whereby we processed all these models 10 times with both methods and reported the averaged times in Table 4.

Table 4. **Time comparison.** Elapsed time of sampling based methods and ours for different model sizes, all timings are averaged over 10 executions. For the brute force sampling method we measure the time using 250, 500 and 1000 candidate views. For the network we measure the average time per model for batch processing 1, 64 and 256 models at the same time. The network approach is faster in orders of magnitude and is independent of the model size as it uses a point cloud of fixed size. We report N/A where the execution did not finish after 12h.

#faces	sampling			ours		
	number of views			batch size		
	250	500	1000	1	64	256
10k	20s	40s	79s	0.263s	0.015s	0.012s
50k	92s	184s	373s	0.253s	0.013s	0.010s
100k	178s	356s	722s	0.260s	0.018s	0.015s
400k	737s	1479s	2929s	0.270s	0.020s	0.017s
1M	2030s	N/A	N/A	0.258s	0.010s	0.007s

While the elapsed time of the sampling approach is approximately linear in the number of candidate views and the number of faces the network only requires one execution. This execution’s time is independent of the model size, outperforming the other method in orders of magnitude. While we see some variation in the execution time of the network, which we account to varying numbers of points in the 3D convolutions and point hierarchy levels, the timings are comparable for all inspected models.

6 LIMITATIONS

To achieve the reported results, we had to train category specific instances of our network in a divide-and-conquer scheme, which

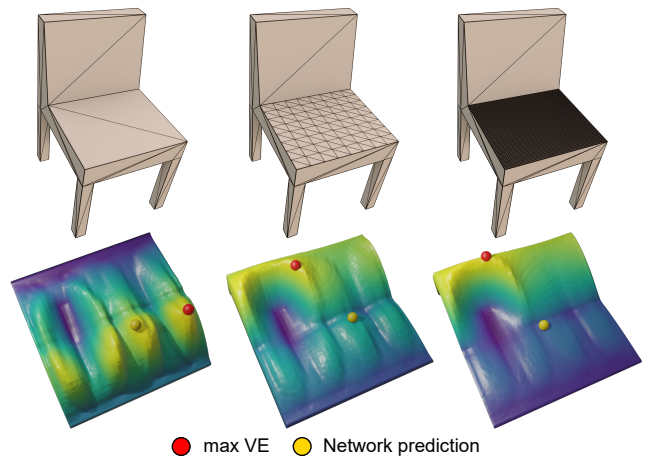


Fig. 11. **Robustness to mesh polygonization.** We show predictions using VE for different subdivisions of the seating surface. As VE favors small triangles the bias towards views from the top increases with higher mesh density (red). Our network based approach remains stable independent of the meshing (yellow).

is common for similar deep learning tasks such as viewpoint estimation [Shi and Tao 2019] or upright prediction [Liu et al. 2016]. This prevents us from generalizing to unseen categories, a way to bypass this problem is through an upstream classification network which classifies the input model to the closest of the trained categories and passes it to the respective category-specific network. Future work might examine including this pre-categorization during training with the goal of geometry specific instead of category specific division to achieve better generalization. To model human preference we limited ourselves to object categories from Pascal3D+ in order to be able to train an image to viewpoint estimator on real labelled data, however other categories could be considered once training viewpoint estimators only on synthetic data [Su et al. 2015] achieves comparable results. The quality of the predictions inherently depends on the viewpoint quality measure used during training. As of now there is no measure that exceeds others in every setting [Bonaventura et al. 2018], we tried to accommodate this fact by showing the applicability for different viewpoint quality measures and expect our proposed network to work with future quality measures as well.

7 CONCLUSION

The proposed neural network provides a way to predict high quality viewpoints for different viewpoint quality measures and model categories, while outperforming the performance of existing techniques by several orders of magnitude. It is able to incorporate informational content from information theoretical measures, human preference from image analysis and natural upright orientation of the model. The proposed dynamic label generation method is essential to resolve label ambiguity during training, outperforming existing methods, and is possibly extendable to other learning tasks that involve label ambiguity. We showed that the output of the network is insensitive to meshing properties, which makes us believe that the network has an internal representation of a clean mesh.

On top of the contributions made in this article, we provide a dataset, which will be, to our knowledge, the first large scale viewpoint quality dataset containing more than 16k models in total, more details can be found in Appendix G.

Future research might investigate the possibility to induce a polygonization bias into the network by exposing it to specifically meshed models during training, e.g., tetrahedral surface meshes or meshes emphasizing certain parts of objects though high density polygons.

REFERENCES

Carlos Andújar, P Vázquez, and Marta Fairén. 2004. WayARFinder: guided tours through complex walkthrough models. *Computer Graphics Forum* 23, 3 (2004), 499–508. <https://doi.org/10.1111/j.1467-8659.2004.00781.x>

Volker Blanz, Michael J Tarr, and Heinrich H Bülthoff. 1999. What object attributes determine canonical views? *Perception* 28, 5 (1999), 575–599.

Xavier Bonaventura, Miquel Feixas, Mateu Sbert, Lewis Chuang, and Christian Wallraven. 2018. A Survey of Viewpoint Selection Methods for Polygonal Models. *Entropy* 20, 5 (2018). <https://doi.org/10.3390/e20050370>

Udeepa D. Bordoloi and Han-Wei Shen. 2005. View selection for volume rendering. In *VIS 05. IEEE Visualization, 2005*. 487–494. <https://doi.org/10.1109/VISUAL.2005.1532833>

Enric Corona, Kaustav Kundu, and Sanja Fidler. 2018. Pose Estimation for Objects with Rotational Symmetry. In *2018 IEEE/RSJ International Conference on Intelligent Robots and Systems (IROS)*. 7215–7222.

Frank Deinzer, Christian Derichs, Heinrich Niemann, and Joachim Denzler. 2006. Integrated Viewpoint Fusion and Viewpoint Selection for Optimal Object Recognition.. In *BMVV*. 287–296.

Frank Deinzer, Christian Derichs, Heinrich Niemann, and Joachim Denzler. 2009. A framework for actively selecting viewpoints in object recognition. *International Journal of Pattern Recognition and Artificial Intelligence* 23, 04 (2009), 765–799. <https://doi.org/10.1142/S0218001409007351>

Yuval Eldar, Michael Lindenbaum, Moshe Porat, and Yehoshua Y. Zeevi. 1997. The farthest point strategy for progressive image sampling. *IEEE Transactions on Image Processing* 6, 9 (Sep. 1997), 1305–1315. <https://doi.org/10.1109/83.623193>

Miquel Feixas, Mateu Sbert, and Francisco González. 2009. A unified information-theoretic framework for viewpoint selection and mesh saliency. *ACM Transactions on Applied Perception (TAP)* 6, 1 (2009), 1.

Sebastian Freitag, Benjamin Weyers, Andrea Bönsch, and Torsten W Kuhlen. 2015. Comparison and Evaluation of Viewpoint Quality Estimation Algorithms for Immersive Virtual Environments. *ICAT-EGVE 15* (2015), 53–60.

Sebastian Freitag, Benjamin Weyers, and Torsten W Kuhlen. 2017. Assisted travel based on common visibility and navigation meshes. In *2017 IEEE Virtual Reality (VR)*. IEEE, 369–370.

Hongbo Fu, Daniel Cohen-Or, Gideon Dror, and Alla Sheffer. 2008. Upright Orientation of Man-made Objects. *ACM Trans. Graph.* 27, 3, Article 42 (Aug. 2008), 7 pages. <https://doi.org/10.1145/1360612.1360641>

Álvaro González. 2010. Measurement of areas on a sphere using Fibonacci and latitude–longitude lattices. *Mathematical Geosciences* 42, 1 (2010), 49.

Stefan Gumhold. 2002. Maximum Entropy Light Source Placement. In *Proceedings of IEEE Visualization Conference*. 275–282. <https://doi.org/10.1109/VISUAL.2002.1183785>

Jingwu He, Linbo Wang, Wenzhe Zhou, Hongjie Zhang, Xiufen Cui, and Yanwen Guo. 2017. Viewpoint Selection for Photographing Architectures. [arXiv:1703.01702](https://arxiv.org/abs/1703.01702)

Julian Heinrich, Jenny Vuong, Christopher J Hammang, Andrew Wu, Markus Rittenbruch, James Hogan, Margot Brereton, and Seán I O’Donoghue. 2016. Evaluating viewpoint entropy for ribbon representation of protein structure. In *Computer Graphics Forum*, Vol. 35. Wiley Online Library, 181–190.

Pedro Hermosilla, Tobias Ritschel, Pere-Pau Vázquez, Alvar Vinacua, and Timo Ropinski. 2018. Monte Carlo convolution for learning on non-uniformly sampled point clouds. In *SIGGRAPH Asia 2018 Technical Papers*. ACM, 235.

Michael Kazhdan, Thomas Funkhouser, and Szymon Rusinkiewicz. 2003. Rotation Invariant Spherical Harmonic Representation of 3D Shape Descriptors. *Proc 2003 Eurographics vol. 43* (07 2003).

Seong-heum Kim, Yu-Wing Tai, Joon-Young Lee, Jaesik Park, and In So Kweon. 2017. Category-Specific Salient View Selection via Deep Convolutional Neural Networks. In *Computer Graphics Forum*, Vol. 36. Wiley Online Library, 313–328.

Diederik Kingma and Jimmy Ba. 2014. Adam: A Method for Stochastic Optimization. *International Conference on Learning Representations* (12 2014).

Chang Ha Lee, Amitabh Varshney, and David W Jacobs. 2005. Mesh saliency. *ACM transactions on graphics (TOG)* 24, 3 (2005), 659–666.

Shuai Liao, Efstratios Gavves, and Cees GM Snoek. 2019. Spherical Regression: Learning Viewpoints, Surface Normals and 3D Rotations on n-Spheres. In *Proceedings of the IEEE Conference on Computer Vision and Pattern Recognition*. 9759–9767.

Cong-Kai Lin and Wen-Kai Tai. 2012. Automatic upright orientation and good view recognition for 3D man-made models. *Pattern Recognition* 45, 4 (2012), 1524 – 1530. <https://doi.org/10.1016/j.patcog.2011.10.022>

Christophe Lino and Marc Christie. 2015. Intuitive and efficient camera control with the toric space. *ACM Transactions on Graphics (TOG)* 34, 4 (2015), 1–12.

Chang-an Liu, Rui-fang Dong, and Hua Wu. 2014. Flying robot based viewpoint selection for the electricity transmission equipment inspection. *Mathematical Problems in Engineering* 2014 (2014). <https://doi.org/10.1155/2014/783810>

Hong Liu, Lei Zhang, and Hua Huang. 2012. Web-image driven best views of 3D shapes. *The Visual Computer* 28, 3 (01 Mar 2012), 279–287. <https://doi.org/10.1007/s00371-011-0638-z>

Zishun Liu, Juyong Zhang, and Ligang Liu. 2016. Upright orientation of 3D shapes with Convolutional Networks. *Graphical Models* 85 (2016), 22 – 29. <https://doi.org/10.1016/j.gmod.2016.03.001> SI CVM 2016 selected Papers.

Eric Marchand and François Chaumette. 1999. Active vision for complete scene reconstruction and exploration. *IEEE Transactions on Pattern Analysis and Machine Intelligence* 21, 1 (1999), 65–72.

Monique Meuschke, Wito Engelke, Oliver Beuing, Bernhard Preim, and Kai Lawonn. 2017. Automatic Viewpoint Selection for Exploration of Time-Dependent Cerebral Aneurysm Data. In *Bildverarbeitung fuer die Medizin 2017*. Springer, 352–357.

Eva Monclús, Pere-Pau Vázquez, and Isabel Navazo. 2012. Efficient selection of representative views and navigation paths for volume data exploration. In *Visualization in Medicine and Life Sciences II*. Springer, 133–151.

Konrad Mühler, Mathias Neugebauer, Christian Tietjen, and Bernhard Preim. 2007. Viewpoint selection for intervention planning.. In *EuroVis*. 267–274.

Dimitri Plemenos and Madjid Benayada. 1996. Intelligent display in scene modeling. new techniques to automatically compute good views. In *International Conference GraphiCon*, Vol. 96. 1–5.

Oleg Polonsky, Giuseppe Patane, Silvia Biasotti, Craig Gotsman, and Michela Spagnuolo. 2005. What’s in an image? Towards the computation of the “best” view of an object. *The Visual Computer* 21 (08 2005), 840–847. <https://doi.org/10.1007/s00371-005-0326-y>

Charles R Qi, Li Yi, Hao Su, and Leonidas J Guibas. 2017. PointNet++: Deep Hierarchical Feature Learning on Point Sets in a Metric Space. arXiv:1706.02413

Joseph Redmon and Ali Farhadi. 2018. YOLOv3: An Incremental Improvement. arXiv:cs.CV/1804.02767

A. Saran, B. Lacic, S. Majumdar, J. Hess, and S. Niekum. 2017. Viewpoint selection for visual failure detection. In *2017 IEEE/RSJ International Conference on Intelligent Robots and Systems (IROS)*. 5437–5444. <https://doi.org/10.1109/IROS.2017.8206439>

Mateu Sbert, Dimitri Plemenos, Miquel Feixas, and Francisco González. 2005. Viewpoint Quality: Measures and Applications. 185–192. <https://doi.org/10.2312/COMPAESTH/COMPAESTH05/185-192>

Adrian Secord, Jingwan Lu, Adam Finkelstein, Manish Singh, and Andrew Nealen. 2011. Perceptual models of viewpoint preference. *ACM Transactions on Graphics (TOG)* 30, 5 (2011), 109.

Thomas W. Sederberg and Scott R. Parry. 1986. Free-form deformation of solid geometric models. *ACM SIGGRAPH computer graphics* 20, 4 (1986), 151–160.

Neng Shi and Yubo Tao. 2019. CNNs Based Viewpoint Estimation for Volume Visualization. *ACM Transactions on Intelligent Systems and Technology (TIIST)* 10, 3 (2019), 27.

Neil Smith, Nils Moehle, Michael Goesele, and Wolfgang Heidrich. 2018. Aerial path planning for urban scene reconstruction: A continuous optimization method and benchmark. In *SIGGRAPH Asia 2018 Technical Papers*. ACM, 183.

Ran Song, Yonghui Liu, Ralph R Martin, and Paul L Rosin. 2014. Mesh saliency via spectral processing. *ACM Transactions on Graphics (TOG)* 33, 1 (2014), 1–17.

Nitish Srivastava, Geoffrey Hinton, Alex Krizhevsky, Ilya Sutskever, and Ruslan Salakhutdinov. 2014. Dropout: A Simple Way to Prevent Neural Networks from Overfitting. *Journal of Machine Learning Research* 15 (2014), 1929–1958. <http://jmlr.org/papers/v15/srivastava14a.html>

Hao Su, Charles R Qi, Yangyan Li, and Leonidas J Guibas. 2015. Render for cnn: Viewpoint estimation in images using cnns trained with rendered 3d model views. In *Proceedings of the IEEE International Conference on Computer Vision*. 2686–2694.

Christian Szegedy, Wei Liu, Yangqing Jia, Pierre Sermanet, Scott Reed, Dragomir Anguelov, Dumitru Erhan, Vincent Vanhoucke, and Andrew Rabinovich. 2015. Going deeper with convolutions. In *2015 IEEE Conference on Computer Vision and Pattern Recognition (CVPR)*. 1–9. <https://doi.org/10.1109/CVPR.2015.7298594>

Roopak R Tamboli, Peter A Kara, Aron Cserkaszky, Attila Barsi, Maria G Martini, and Soumya Jana. 2018. Canonical 3D object orientation for interactive light-field visualization. In *Applications of Digital Image Processing XLI*, Vol. 10752. International Society for Optics and Photonics, 107520A.

Yubo Tao, Hai Lin, Hujun Bao, Feng Dong, and Gordon Clapworthy. 2009. Structure-aware viewpoint selection for volume visualization. In *2009 IEEE Pacific Visualization Symposium*. IEEE, 193–200.

Pere-Pau Vázquez, Miquel Feixas, Mateu Sbert, and Wolfgang Heidrich. 2001. Viewpoint selection using viewpoint entropy. In *VMV*, Vol. 1. 273–280.

Pere-Pau Vázquez, Miquel Feixas, Mateu Sbert, and Antoni Llobet. 2002. Viewpoint entropy: a new tool for obtaining good views of molecules. In *ACM International Conference Proceeding Series*, Vol. 22. 183–188.

Pere-Pau Vázquez, Timo Götzelmann, Knut Hartmann, and Andreas Nürnberg. 2008. An interactive 3D framework for anatomical education. *International journal of computer assisted radiology and surgery* 3, 6 (2008), 511–524.

Ivan Viola, Miquel Feixas, Mateu Sbert, and Meister Eduard Groller. 2006. Importance-driven focus of attention. *IEEE Transactions on Visualization and Computer Graphics* 12, 5 (2006), 933–940.

Zhirong Wu, Shuran Song, Aditya Khosla, Fisher Yu, Linguang Zhang, Xiaoou Tang, and Jianxiong Xiao. 2015. 3d shapenets: A deep representation for volumetric shapes. In *Proceedings of the IEEE conference on computer vision and pattern recognition*. 1912–1920.

Yu Xiang, Roozbeh Mottaghi, and Silvio Savarese. 2014. Beyond pascal: A benchmark for 3d object detection in the wild. In *IEEE Winter Conference on Applications of Computer Vision*. IEEE, 75–82.

Changhe Yang, Yanda Li, Can Liu, and Xiaoru Yuan. 2019. Deep learning-based viewpoint recommendation in volume visualization. *Journal of Visualization* 22, 5 (01 Oct 2019), 991–1003. <https://doi.org/10.1007/s12650-019-00583-4>

Wang Yanni Zheng Yao. 2008. Intelligent Volume Visualization through Transfer Function and Viewpoint Selection [J]. *Journal of Computer-Aided Design & Computer Graphics* 5 (2008).

Table 5. **Viewpoint estimation.** Category wise comparison of the test scores for different configurations of spherical regression. We compare a shared convolutional block for the six categories to category specific convolutional blocks. Category specific training leads to best results on median error and higher level accuracy. We also report results from Liao et al. [Liao et al. 2019].

	conv. block	plane	bottle	car	chair	table	sofa
Med Err	Liao et al.	9.2	7.3	4.8	8.2	8.5	8.7
	shared(6)	10.3	7.6	4.7	8.6	13.3	8.2
	cat. spec.	6.9	6.7	4.2	7.0	7.1	6.4
Acc@ $\pi/6$	Liao et al.	88	96	93	93	74	98
	shared(6)	87	96	92	90	70	93
	cat. spec.	93	94	94	92	70	95
Acc@ $\pi/12$	Liao et al.	N/A	N/A	N/A	N/A	N/A	N/A
	shared(6)	33	48	72	44	30	45
	cat. spec.	54	58	78	54	57	58

A VIEWPOINT ESTIMATION FROM IMAGES

To retrieve the viewpoints from the processed images in Section 3.2 we use a spherical regression network [Liao et al. 2019]. While the original authors use a shared convolutional block over all categories which allows them to have one network for many categories, we found that separate convolutional blocks achieve better performance, at least on the categories we are interested in. We retrained category specific instances for the viewpoint estimation networks using the same hyperparameters as reported in the original paper, except for the batch size which we half because of hardware constraints. Training was performed on the Pascal3D+ dataset [Xiang et al. 2014] and synthetic data [Su et al. 2015]. We stop training after 20k or 40k epochs, dependent on the size of the dataset, to prevent overfitting. In Table 5 we compare training a shared convolutional block for our six categories, category specific convolutional blocks to the results reported by Liao et al. [Liao et al. 2019]. The category specific approach achieves best results on median error and higher level accuracy scores at almost the same lower level accuracy.

B VALIDATION OF THE ELEVATION DENSITY ESTIMATION

To validate our viewpoint estimation routine we collect images from a second independent image source, namely www.pexels.com. We perform a KDE for both image sources and measure the Kullback-Leibler divergence

$$D(\tilde{f}_f \| \tilde{f}_p) = \int_{-\pi}^{\pi} \tilde{f}_f(x) \log \frac{\tilde{f}_f(x)}{\tilde{f}_p(x)} dx,$$

between the estimated densities \tilde{f}_f for flickr and \tilde{f}_p for pexels. The integration is approximated by sampling 1k equidistant points in $[-\pi, \pi]$. Between the results from the two image sets the KL divergence is smaller than 0.05 for five of the six categories:

	plane	bottle	car	chair	table	sofa
KL-divergence	0.129	0.004	0.007	0.030	0.041	0.036

Table 6. **Detailed results.** Breakdown from Table 1 for each category.

		airplane	bench	bottle	car	chair	sofa	table	toilet	mean
VR	SL	71.4	71.7	69.9	65.1	72.4	76.4	76.4	64.9	71.0
	SR	71.0	73.4	72.2	69.3	65.3	59.2	80.3	67.4	69.8
	ML	63.2	73.6	70.0	74.2	77.5	73.3	81.0	64.0	72.1
	GL	66.2	83.0	69.1	78.6	75.5	75.5	80.8	72.4	75.1
	ML+GL	74.8	72.8	78.0	80.3	77.9	75.7	82.0	84.3	78.2
VE	SL	60.7	50.9	64.8	58.0	63.8	88.7	38.3	74.4	62.4
	SR	49.4	65.1	53.3	64.0	66.3	63.4	73.5	70.0	63.1
	ML	55.4	62.1	50.4	79.8	73.9	83.3	76.4	79.2	70.1
	GL	70.0	69.5	52.9	82.0	71.7	87.9	76.6	83.4	74.2
	ML+GL	79.1	67.7	75.3	84.0	73.0	88.8	83.0	83.8	79.3
VKL	SL	89.2	76.2	74.9	83.7	83.5	86.3	86.0	65.6	80.7
	SR	86.2	84.4	88.9	74.0	72.1	79.1	89.0	71.5	80.6
	ML	79.7	79.8	92.7	80.4	86.2	75.5	90.2	76.5	82.6
	GL	91.8	88.1	90.9	85.3	89.3	94.0	90.9	84.4	89.3
	ML+GL	95.2	85.5	94.9	89.7	90.8	92.2	91.6	89.8	91.2
VMI	SL	90.6	79.2	80.4	84.0	88.3	92.6	84.3	64.4	83.0
	SR	85.0	86.2	86.5	81.6	70.6	75.7	91.1	64.0	80.1
	ML	88.7	68.7	92.1	80.2	89.9	81.9	87.7	67.8	82.1
	GL	94.0	85.1	91.5	78.7	91.0	91.2	88.8	81.7	87.7
	ML+GL	96.6	87.3	94.1	92.2	93.0	93.5	90.1	93.4	92.5

The category *airplane* has a slightly higher KL divergence, which we contribute to a wider range of perceived elevations, see blue plot in Fig. 4. We conclude that our estimated densities inherit no significant bias from the used image source.

C MESH CLEANING PIPELINE

Our mesh cleaning pipeline consists of three steps. First we resolve self intersections of the mesh, using PyMesh. These are particularly bad as in this case the area of a face does not correspond to its potentially visible area, as parts of a face can be hidden inside the model, changing the values of A_z and A_t . As a second step we

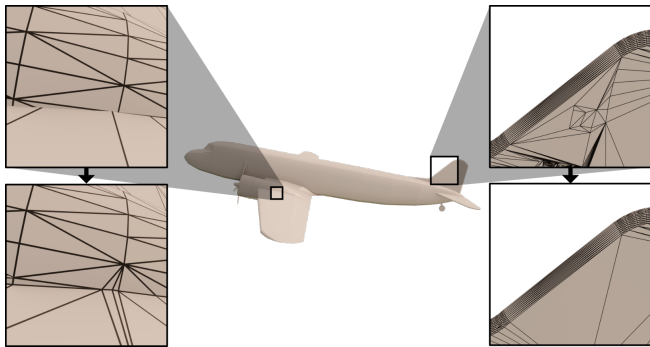


Fig. 12. **Mesh cleaning.** Results of the different steps to clean the meshes on *airplane_0004*. The original mesh contains self intersections (left) and non-uniform meshing artifacts (right), which are resolved in the first and third step our mesh cleaning pipeline, respectively.

remove non-surface polygons by computing the visibility of the faces from 1000 views and drop all non-visible faces of the model using MeshLab. This is primarily done to create cleaner surface meshes by removing unwanted parts of the model, e.g. passenger seats inside planes. This results in a A_t being closer to the actual surface area of the model, while also speeding up the downstream tasks by reducing the number of polygons per model. As the first step introduces artifacts in the form of small and irregular meshing, where self-intersections were resolved, we add a third and last step where we regularize the surface meshes by performing an edge-collapse reduction algorithm, again using MeshLab. Furthermore, the last step also removes unwanted structures in the meshes, e.g. polygons referring to different textures, which are not relevant for shape information but can influence the viewpoint quality. Fig. 12 shows details of the model *airplane_0004* from ModelNet40, which contains self-intersections (top left) and unnecessary polygons (top right). The proposed mesh processing resolves self-intersections in the first step and cleans the meshing in the third step (bottom images).

D SYMMETRY PRESERVING DEFORMATIONS

For each dimension we place four equidistant control points on the bounding box of the model. For one half of the control point displacements are sampled from a Gaussian distribution with variance $1/12$ the size of the bounding box and clip the absolute value of the displacement at $1/8$ of the bounding box to prevent degeneration of the model. The displacement is then mirrored onto the second

Table 7. **Detailed results.** Breakdown from Table 2 for each category.

		airplane	bench	bottle	car	chair	sofa	table	toilet	mean
VR + S	$SO(3)$	81.7	62.6	65.7	49.2	81.8	69.5	78.2	49.7	67.3
	$SO(3)$, predicted up	87.7	79.4	86.6	70.7	81.6	76.2	80.3	62.0	78.0
	fixed up	94.3	89.4	91.7	78.3	90.0	87.9	85.3	88.2	88.1
VE + S	$SO(3)$	88.5	68.7	69.1	65.4	80.1	83.0	81.2	50.4	73.3
	$SO(3)$, predicted up	92.2	73.6	90.3	92.6	83.2	84.8	82.1	66.6	83.2
	fixed up	95.5	89.4	97.3	92.6	91.4	94.4	90.8	93.2	93.1
VKL + S	$SO(3)$	74.5	48.0	78.2	54.5	78.2	77.8	68.1	47.0	65.8
	$SO(3)$, predicted up	86.8	66.3	90.6	82.1	78.8	83.4	76.1	64.0	78.5
	fixed up	89.6	83.3	96.8	83.4	87.3	93.8	81.4	87.1	87.8
VMI + S	$SO(3)$	73.1	43.6	71.5	54.0	78.9	80.2	76.2	42.5	65.0
	$SO(3)$, predicted up	88.0	67.7	90.7	79.3	78.5	82.0	73.6	55.9	77.0
	fixed up	90.1	81.2	97.2	80.9	89.2	91.4	83.5	83.7	87.1

Table 8. **Up vector estimation results.** Mean cosine distance and accuracy of the predicted vectors on the test set, we evaluated the SL and SR approach.

category	cos. dist.		Acc@ $\pi/6$	
	SR	SL	SR	SL
airplane	0.04	0.02	96	96
bench	0.43	0.19	31	73
bottle	0.14	0.06	93	95
car	0.10	0.03	96	87
chair	0.30	0.03	61	91
sofa	0.16	0.18	81	72
table	0.01	0.02	100	97
toilet	0.21	0.04	47	90
mean	0.21	0.07	75	88

half of the control points to preserve model symmetry. The overall deformation of the model is then computed per point by linear interpolation of the displacements of the control points, see Fig. 13.

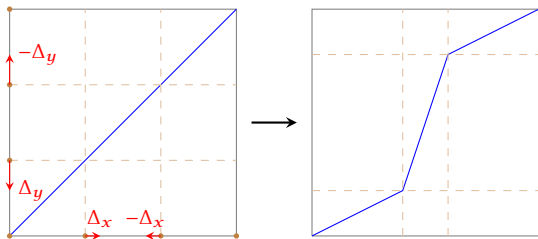


Fig. 13. **Symmetry preserving deformation.** Uniformly distributed control points are displaced with a clipped Gaussian noise which is mirrored along the symmetry axes. The intermediate spaces are deformed with linear interpolation of the displaced control points.

E UPRIGHT ORIENTATION PREDICTION

We compared both the SL and the SR method for the up vector regression and found that SL achieves better overall results, as shown in the test scores in Table 8. We suppose SR provides no benefits in this setting, as the categories we consider have no top-bottom symmetry.

F VIEWPOINT PREDICTION

Tables 6 and 7 show the test results on the different categories for the experiments from Sections 5.2 and 5.4. Our combined ML+GL method achieves best performance on almost all categories and viewpoint quality measures. The results are comparable on all categories for all viewpoint quality measures, with or without considering statistics. We see a correlation between the performance gap from *predicted up* to *fixed up* in Table 7 and the performance of the up vector estimation in Table 8, as mentioned in Section 5.4.

G DATASET

We release our training data which contains dense viewpoint quality values for 1k viewpoints on a Fibonacci sphere for VR, VE, VKL and VMI for ~12k models from ModelNet40. For a subset of ~4k models from the categories *airplane*, *bench*, *bottle*, *car*, *chair*, *sofa*, *table* and *toilet* we additionally provide the cleaned models using our pipeline together with the sampled viewpoint quality values for VR, VR + S, VE, VE + S, VKL, VKL + S, VMI and VMI + S.